Behavior of Boron Trifluoride in Cryosolutions: A Combined ab Initio, Monte Carlo, and FTIR Investigation

W. A. Herrebout and B. J. van der Veken*

Contribution from the Department of Chemistry, Universitair Centrum Antwerpen, Groenenborgerlaan 171, B-2020 Antwerpen, Belgium

Received February 24, 1998

Abstract: Solutions of BF_3 in liquefied Ar, N_2, and Ar/N_2 mixtures have been investigated using Monte Carlo simulations and infrared cryospectroscopy. The simulations show that in pure liquefied Ar only solvation of BF_3 occurs, but that in solutions that contain N_2, also van der Waals complexes of the types $BF_3{\cdot}N_2$ and $N_2{\cdot}BF_3{\cdot}N_2$ are formed. The fractions of monomer and complexes are calculated to vary with temperature and with concentration of N_2. In the infrared spectra of BF_3 dissolved in liquid Ar/N_2 mixtures, the BF_3 bands have complex structures, which in the case of ν_3 clearly resolve into triplets. This is attributed to the formation of 1:1 and 1:2 complexes of BF_3 with N_2 molecules. The evolution of the relative intensities of the components of the BF_3 multiplets as a function of temperature and as a function of concentration agree with the Monte Carlo predictions. From a temperature-dependent study, the complexation enthalpy for $BF_3{\cdot}N_2$ in liquefied argon was determined to be $-4.8(5)$ kJ mol^{-1}.

Introduction

One of the fields in which ab initio methods have recently expanded is in the calculation of the wave function of molecules in solution.[1−11] These methods include for instance the self-consistent isodensity polarizable continuum model (SCIPCM),[7] in which the solvent is treated as a polarizable continuum characterized by its relative permittivity κ. Isolated argon atoms show no electrical multipoles, and hence, argon as well as other liquefied rare gases are the closest a solvent can approach a continuum. Therefore, calculations of this type open interesting perspectives for the study of van der Waals molecules in cryosolution,[12−15] where solvents such as liquefied argon (LAr) are being used.

Temperature-dependent infrared spectroscopy of cryosolutions containing chemical equilibria in which van der Waals complexes are formed allows the measurement of the complexation enthalpy $\Delta H°$. This technique allows enthalpies well below 10 kJ mol^{-1} to be measured. Because of the thermodynamic implications, these enthalpies are not a direct measure of the stability of the isolated complex and cannot be directly compared with vapor-phase data, either experimental or calculated by ab initio methods, on the same complex. To obtain stabilities of isolated complexes from solution data, corrections for solvent influences based on SCIPCM calculations have been described,[16] and the results appear to be promising.[17−22] However, the application of this approach to studies in cryosolvents other than rare gases is not self-evident. In fact, there are indications that continuum solvent models are doomed to fail in the case of solutions in liquid nitrogen (LN_2), which can be seen from the following considerations. The relative permittivity of liquid nitrogen differs but marginally from that of liquid argon. Therefore, SCIPCM calculations predict very similar solvent stabilizations for a species dissolved in LAr or in LN_2. Consequently, complexation enthalpies in LAr and LN_2 should be quite similar. However, the $\Delta H°$ in LN_2 for van der Waals complexes involving BF_3 as Lewis acid are consistently ∼4.5 kJ mol^{-1} smaller than in LAr.[17,22] Also, for complexes using HCl as Lewis acid, a lower $\Delta H°$ in LN_2 compared to LAr has been observed[12,16] albeit that the difference is significantly smaller. These data show there is a specific interaction between the nitrogen molecules of the solvent and the Lewis acid. Such an interaction may take the form of a van der Waals complex

(1) Tomasi, J.; Persico, M. *Chem. Rev.* **1994**, *94*, 2027.
(2) Cammi, R.; Tomasi, J. *J. Chem. Phys.* **1994**, *100*, 7495.
(3) Cammi, R.; Tomasi, J. *J. Chem. Phys.* **1994**, *101*, 3888.
(4) Fortunelli, A.; Tomasi, J. *Chem. Phys. Lett.* **1995**, *231*, 34.
(5) Cossi, M.; Tomasi, J.; Cammi, R. *Int. J. Quantum Chem.* **1995**, *29*, 695.
(6) Cossi, M.; Barone, V.; Cammi, R.; Tomasi, J. *Chem. Phys. Lett.* **1996**, *255*, 327.
(7) Foresman, J. B.; Keith, T. A.; Wiberg, K. B.; Snoonian, J.; Frisch, M. J. *J. Phys. Chem.* **1996**, *100*, 16098.
(8) Cances, E.; Mennucci, B.; Tomasi, J. *J. Chem. Phys.* **1997**, *107*, 3032.
(9) Pomelli, C. S.; Tomasi, J. *Theor. Chem. Acc.* **1997**, *96*, 39.
(10) Floris, F. M.; Selmi, M.; Tani, A.; Tomasi, J. *J. Chem. Phys.* **1997**, *107*, 6353.
(11) Foresman, J. B.; Frisch, Æ. *Exploring Chemistry with Electronic Structure Methods: A Guide to Using Gaussian*, 2nd ed.; 1997; p 144.
(12) Kimmel'fel'd, Ya. M. In *Vibrational Spectra and Structure*; Durig, J. R., Ed.; Elsevier: Amsterdam, 1992; Vol. 19.
(13) Tokhadze, K. G.; Tkhorzheskaya, N. A. *J. Mol. Struct.* **1992**, *270*, 351.
(14) Tokhadze, K. G. In *Molecular Cryospectroscopy*; Clark, R. J. H., Hester, R. E., Eds.; Advances in Spectroscopy 23; Wiley: Chichester, 1995; p 136.
(15) Van der Veken, B. J. In *Low Temperature Molecular Spectroscopy*; Fausto, R., Ed.; Kluwer Academic Publishers: Dordrecht, 1996.
(16) Herrebout, W. A.; Everaert, G. P.; Van der Veken, B. J.; Bulanin, M. O. *J. Chem. Phys.* **1997**, *107*, 8886.
(17) Herrebout, W. A.; Van der Veken, B. J. *J. Am. Chem. Soc.* **1997**, *119*, 10446.
(18) Van der Veken, B. J.; Sluyts, E. J. *J. Phys. Chem. A* **1997**, *101*, 9070.
(19) Everaert, G. P.; Herrebout, W. A.; Van der Veken, B. J.; Lundell, J.; Räsänen, M. *Chem. Eur. J.* **1998**, 4, 321.
(20) Van der Veken, B. J.; Sluyts, E. J.; Herrebout, W. A. *J. Mol. Struct.* **1998**, *449*, 219.
(21) Herrebout, W. A.; Van der Veken, B. J. *J. Mol. Struct.* **1998**, *449*, 23.
(22) Stolov, A. A.; Herrebout, W. A., Van der Veken, B. J. *J. Am. Chem. Soc.* **1998**, *120*, 7310.

S0002-7863(98)00626-X CCC: $15.00
Published on Web 09/11/1998

between the solute and one or more solvent molecules: for solutions of HCl in LN_2 in the infrared spectra separate bands attributed to monomer HCl and HCl·N_2 have been identified,[14] providing evidence for the occurrence of an equilibrium of the type:

$$HCl + N_2 \rightleftharpoons HCl\cdot N_2$$

However, for solutions of BF_3 in LN_2, such a splitting of spectral bands, supporting an analogous equilibrium, is not immediately obvious. Thus, while the occurrence of a complex between BF_3 and N_2 in vapor-phase molecular beams is well-documented,[23] the formation of similar complexes in LN_2 solutions is an open question. It is the purpose of this study to analyze the behavior of BF_3 in cryosolutions in more detail. To this end we have performed Monte Carlo simulations, using intermolecular potentials taken from the literature and from ab initio calculations, of BF_3 dissolved in LN_2, LAr, and mixtures of LN_2 and LAr. Also, we have studied, at different temperatures, the infrared spectra of solutions in BF_3 in mixtures of LN_2 and LAr. The combined results give convincing evidence for the formation of van der Waals molecules between BF_3 and N_2 in these solutions, as will become clear from the following paragraphs.

Experimental Section

Ab Initio Calculations. Unless stated otherwise, the ab initio calculations were performed using Gaussian 94.[24] For all calculations, the correlation energy was calculated using Møller−Plesset perturbation theory at the second order, including explicitly all electrons, while the Berny optimization[25] was used with the tight convergence criteria. For all calculations, as a compromise between accuracy and applicability to larger systems, the 6-31+G* basis set was used.

Monte Carlo Simulations. The Monte Carlo simulations were carried out in the NVT ensemble, using a sample of 1 solute (BF_3) and 120 solvent (Ar and/or N_2) molecules. All calculations were made in the pair potential approximation. During the calculations, periodic boundary conditions were employed by embedding the cube in an infinite net of cubes with identical composition and configuration, while the intermolecular interactions were computed using a spherical cutoff of 0.95L, where *L* is the box length. For all calculations, the Metropolis algorithm was employed. Equilibrium runs were performed for 250 000 cycles, followed by data collection for 1 250 000 (pure Ar or N_2 solutions) or 1 500 000 (mixtures of Ar and N_2) cycles. In each cycle, new configurations were generated by serially selecting the solvent molecules and changing, at random, their coordinates. In general, a translation in all three coordinates and a rotation modifying the Eulerian angles were carried out, using a procedure similar to that described in ref 26. During the sample part of the runs, the configuration was stored every 25 cycles, yielding 50 000 and 60 000 configurations for the pure solutions and for the mixed solutions, respectively. These configurations were used to examine the structure of the solution in the neighborhood of the solute molecule.

Infrared Spectra. The sample of boron trifluoride (CP grade) was purchased from Union Carbide. The solvent gases, Ar and N_2, were supplied by L′Air Liquide and have a stated purity of 99.9999%. In the vapor-phase spectra of argon and nitrogen, no impurities could be detected, while small amounts of SiF_4 were present as an impurity in the BF_3 used. All gases were used without further purification.

The infrared spectra were recorded on a Bruker IFS 66v or a Bruker 113v Fourier transform spectrometer, using a Globar source in combination with a Ge/KBr beam splitter and a broad-band MCT detector. The interferograms were averaged over 200 scans, Happ Genzel apodized, and Fourier transformed using a zero filling factor of 4, to yield spectra at a resolution of 0.5 cm^{-1}. A detailed description of the liquid noble gas setup, containing a cell with an optical path length of 4.0 cm, has been given in a previous study.[15]

Results

Ab Initio Calculations. For $BF_3\cdot N_2$, the microwave data[23] show that the N_2 molecule interacts head-on with the boron atom, the axis of N_2 coinciding with the 3-fold axis of BF_3. In the complex, the planarity of BF_3 is hardly disturbed. This situation is closely analogous to that for the complexes between BF_3 and CO.[27] For the latter also the formation of a 1:2 complex, with one CO on either side of BF_3, has been observed in cryosolution, and a similar complex must be envisaged using N_2 as Lewis base. As no experimental evidence for such a complex was found in the literature, its possible formation was investigated using MP/6-31+G* ab initio calculations. Calculations on the 1:1 complex have been described before,[28,29] but the published data do not include vibrational frequencies, which are of interest to the present study. Therefore, calculations were also made, for the 1:1 complex with the extra advantage that structures and stabilities obtained at the same level for both complexes can be compared.

The calculations confirm that the 1:2 complex $N_2\cdot BF_3\cdot N_2$, with both N_2 molecules along the C_3 axis of BF_3, is a stable minimum in the energy hypersurface. Its optimized geometry and complexation energy are compared with those for the 1:1 complex in Table 1.

During the formation of the 1:2 complex a weak anti-cooperative effect is active, as the complexation energy of the 1:2 complex is ∼1.8% smaller than twice the value for the 1:1 complex. This effect also shows in the B···N bond lengths, which in the 1:2 complex are slightly larger than in the 1:1 complex. The natural bond orbital partioning scheme[30] applied to $BF_3\cdot N_2$ results in a charge transfer of 0.0095*e* from N_2 to BF_3, and of 0.0100*e* from each N_2 to BF_3 in $N_2\cdot BF_3\cdot N_2$. These charge transfers, combined with donor−acceptor theory,[31] readily explain the minor structural changes in the monomers upon complexation. The smallness of the transfers suggests

(23) Janda, K. C.; Bernstein, L. S.; Steed, J. M.; Novick, S. E., Klemperer, W. *J. Am. Chem. Soc.* **1978**, *100*, 8074.

(24) Gaussian 94, Revision B.2. Frisch, M. J.; Trucks, G. W.; Schlegel, H. B.; Gill, P. M. W.; Johnson, B. G.; Robb, M. A.; Cheeseman, J. R.; Keith, T.; Petersson, G. A.; Montgomery, J. A.; Raghavachari, K.; Al-Laham, M. A.; Zakrzewski, V. G.; Ortiz, J. V.; Foresman, J. B.; Cioslowski, J.; Stefanov, B. B.; Nanayakkara, A.; Challacombe, M.; Peng. C. Y.; Ayala, Y.; Chen, W.; Wong, M. W.; Andres, J. L.; Replogle, E. S.; Gomperts, R.; Martin, R. L.; Fox, D. J.; Binkley, J. S.; Defrees, D. J., Baker, J.; Stewart, J. P.; Head-Gordon, M.; Gonzalez, C.; Pople, J. A. Gaussian, Inc., Pittsburgh, PA, 1995.

(25) Peng, C.; Ayala, P. Y., Schlegel, H. B.; Frisch, M. J. *J. Comput. Chem.* **1996**, *17*, 49.

(26) Allen, M. P.; Tildesley, D. J. *Computer Simulation of Liquids*; Clarendon Press: Oxford, 1987; p 131.

(27) Sluyts, E. J.; Van der Veken, B. J. *J. Am. Chem. Soc.* **1996**, *118*, 440.

(28) Garcia-Leigh, A.; Murell, J. N. *Croat. Chem. Acta* **1984**, *57*, 879.

(29) Nxumalo, L. M.; Andrzejak, M.; Ford, T. A. *J. Chem. Inf. Comput. Sci.* **1996**, *36*, 377.

(30) Reed, A. E.; Curtiss, L. A.; Weinhold, F. *Chem. Rev.* **1988**, *88*, 899.

(31) Gutman, V. *The Donor−Acceptor Approach to Molecular Interactions*; Plenum Press: New York, 1988.

Table 1. MP2/6-31+G* Structural Parameters,[a] Energies and Complexation Energies for N_2, BF_3, $BF_3{\cdot}N_2$, and $N_2{\cdot}BF_3{\cdot}N_2$

	N_2 ($C_{\infty v}$)	BF_3 (D_{3h})	$BF_3{\cdot}N_2$ (C_{3v})	$BF_3{\cdot}(N_2)_2$ (D_{3h})
$r(N_e{\equiv}N_b)$	1.1299		1.1293	1.1293
r(B−F)		1.3259	1.3268	1.3272
$r(B{\cdots}N_b)$			2.7717	2.8035
$\angle(N_b{\cdots}B{-}F)$			90.70	90.00
μ/D	0.00	0.00	0.40	0.00
E/hartree	−109.268694	−323.818962	−433.092294	−542.365464
ΔE/kJ mol^{-1}			−12.18	−23.93

[a] Bond lengths in Å, and bond angles in degrees.

Table 2. MP2/6-31+G* Vibrational Frequencies (cm^{-1}) and Infrared Intensities (km mol^{-1}) for N_2,[a] BF_3, $BF_3{\cdot}N_2$, and $N_2{\cdot}BF_3{\cdot}N_2$

		$^{10}BF_3$		$^{10}BF_3{\cdot}N_2$		$^{11}BF_3$		$^{11}BF_3{\cdot}N_2$	
		$\bar{\nu}$	int	$\bar{\nu}$	int	$\bar{\nu}$	int	$\bar{\nu}$	int
A_1	ν^{N_2}			2183.3	0.5			2183.3	0.5
	$\nu_1^{BF_3}$	873.5		870.9	0.7	873.5		870.9	0.6
	$\nu_2^{BF_3}$	727.6	127.2	708.6	193.2	699.0	118.3	681.0	178.1
	B···N stretch			85.4	0.7			85.2	0.7
E	$\nu_3^{BF_3}$	1498.4	1049.1	1495.2	987.9	1445.3	966.9	1442.1	911.2
	$\nu_4^{BF_3}$	474.3	29.5	476.0	26.1	472.4	30.2	474.1	26.8
	B···N≡N deformation			136.5	0.2			136.4	0.2
	F−B···N deformation			58.6	0.0			58.6	0.0

		$N_2{\cdot}^{10}BF_3{\cdot}N_2$		$N_2{\cdot}^{11}BF_3{\cdot}N_2$	
		$\bar{\nu}$	int	$\bar{\nu}$	int
A_1'	ν^{N_2}	2182.5		2182.5	
	$\nu_1^{BF_3}$	868.9		868.9	
	B···N sym stretch	71.0		71.0	
A_2'	ν^{N_2}	2182.6	0.7	2182.6	0.7
	$\nu_2^{BF_3}$	691.9	266.5	665.1	245.5
	B···N asym stretch	93.9	1.7	93.5	1.7
E'	$\nu_3^{BF_3}$	1492.6	934.6	1439.5	862.5
	$\nu_4^{BF_3}$	476.5	23.3	474.6	24.0
	B···N≡N sym deformation	123.0	0.3	123.0	0.3
	F−B···N sym deformation	29.0	0.1	28.9	0.1
E''	F−B···N asym deformation	140.4		140.4	
	B···N≡N asym deformation	70.1		70.1	

[a] The calculated N≡N stretching frequency of monomer N_2 is 2177.9 cm^{-1}.

that the stability of the complexes in the first place is determined by electrostatic contributions. This, in view of the high net atomic charges in BF_3,[32] is not surprising.

The harmonic frequencies and infrared intensities predicted for monomers and complexes are compiled in Table 2. These data will be discussed in a later paragraph, in connection with the observed frequencies.

Finally, it may be noted that a relatively large dipole moment of 0.40 D was calculated for $BF_3{\cdot}N_2$. This value compares favorably with the experimental value of 0.35(2) D,[23] and the value of 0.366 D reported by Fowler and Stone.[32]

Monte Carlo Simulations. For the argon−argon interaction, several pair potentials have been reported.[33] The Lennard-Jones (LJ) potential, however, remains extensively used and was adopted in this study. The value for the well depth ϵ and for the distance parameter σ are given in Table 3. This table also contains the parameters for the LJ potentials described below.

The potential model for the Ar−N_2 interactions consisted of two LJ functions, one between Ar and each of the N atoms.

The N_2−N_2 interactions were described by a sum of LJ and electrostatic terms. A total of four LJ functions were used, one between each pair of nonbonded N atoms. The electrostatic contributions were calculated using the partial charge model of Murthy.[34] In this model, a charge of −2.3794e is situated at the bond midpoint, while charges of 5.2366e and −4.0469e were situated at the nuclei and at points ∼0.10 A beyond them.

Table 3. Lennard-Jones Parameters Used in the Monte Carlo Simulations

atom 1	atom 2	ϵ/cm^{-1}	σ/Å	ref
Ar	Ar	86.1	3.42	36
Ar	N	46.4	3.36	36
N	N	25.8	3.31	36
Ar	B	54.2	3.04	35
Ar	F	49.2	3.23	35
N	B	35.2	3.68	this study
N	F	29.0	3.04	this study

The potential energy between BF_3 and Ar was described by four LJ functions, one for the Ar−B interaction and one each for the Ar−F interactions. The parameters given in Table 3 were obtained by fitting LJ functions to a CCSD/aug-cc-pVTZ potential energy surface.[35]

Finally, the interactions between BF_3 and N_2 were modeled using a sum of LJ and electrostatic terms. One LJ function was used for the interaction between each atom of N_2 with each atom of BF_3. As no literature data are available on these potentials, the values for the LJ parameters in Table 3 were

(32) Fowler, P. W.; Stone, A. J. *J. Phys. Chem.* **1987**, *91*, 509.
(33) Hirst, D. M. *A Computational Approach to Chemistry*; Blackwell Scientific Publications: Oxford, 1990; p 372.
(34) Murthy, C. S.; O'Shea, S. F.; MacDonald, I. R. *Mol. Phys.* **1983**, *50*, 53.
(35) Herrebout, W. A.; Van der Veken, B. J., unpublished results.

Table 4. RHF/6-311+G** Distributed Multipoles[a] for Boron Trifluoride

atom	x	z	R_{00}	R_{11c}	R_{11s}	R_{20}	R_{21c}	R_{22c}
B	0.000	0.000	1.3434	0.0000	0.0000	−0.2530	0.0000	−0.4381
F_1	0.000	2.509	−0.3210	0.0000	−0.0389	0.1803	0.0000	−0.0071
F_2	2.173	−1.255	−0.3210	−0.0337	0.0195	−0.0271	−0.1383	0.1126
F_3	−2.173	−1.255	−0.3210	0.0337	0.0195	−0.0271	0.1383	0.1126
B−F_1	0.000	1.255	−0.1268	0.0000	−0.0518	0.1487	0.0000	0.0756
B−F_2	1.087	−0.627	−0.1268	−0.0448	0.0259	0.0305	−0.0788	0.1438
B−F_3	−1.087	−0.627	−0.1268	0.0448	0.0259	0.0305	0.0788	0.1438

[a] Using the spherical harmonic notation of ref 38. All values given in atomic units. Because of symmetry, for all expansion points the values for R_{10}, R_{21s}, and R_{22} are equal to zero.

Table 5. Intermolecular Distance ($R_{B\cdots X}$) and Dissociation Energy (D_e) for the BF_3·N_2 and BF_3·Ar van der Waals Complexes

	model potential[a]	exptl values
BF_3·Ar		
$R_{B\cdots Ar}$/Å	3.39	3.325(10)[b]
D_e/kJ mol^{-1}	2.40	
BF_3·N_2		
$R_{B\cdots N}$/Å	2.70	2.886(5)
D_e/kJ mol^{-1}	7.27	7.3(1)[a]

[a] This study. [b] Taken from ref 23.

calculated using the Lorentz−Bertholet mixing rules.[36] No accurate description of the electrostatic contribution was obtained by using a partial charge model for BF_3 and N_2. Therefore, a hybrid procedure was followed, using a distributed multipole model for BF_3 and the above partial charge model for N_2. Although a distributed multipole description for BF_3 has been published,[32] for the present case, the multipoles were calculated, using the Gamess-US program,[37] at the RHF/6-311+G** level, using the nuclei and bond midpoints as expansion points. The results, using the nomenclature of ref 38 for the multipoles, are collected in Table 4. From these, the electrostatic potential around BF_3 was calculated using the formulas given in ref 39.

The accuracy of the potentials was tested by calculating the equilibrium intermolecular distance and the dissociation energy for BF_3·Ar and BF_3·N_2. The results are compared with experimental data in Table 5. The experimental complexation energy quoted for BF_3·N_2 was derived from the complexation enthalpy in LAr as described below. It is clear that the intermolecular distance for BF_3·Ar and the interaction energy for BF_3·N_2 are in good agreement with experiment. The intermolecular distance calculated for the latter, however, is slightly underestimated. The model describing the BF_3−N_2 interaction is a relatively simple one, certainly in the light of the approach followed by Fowler and Stone.[32] However, the simplified description used here a posteriori appears to be justified by the agreement with experiment shown in Table 5.

The results of the simulations for BF_3 in pure LAr at 88 K and in pure LN_2 at 80 K are shown in Figure 1, using two different representations: panels a and c give the classical radial distribution function $g(R)$, and in panels b and d a two-dimensional distribution function $g(R,\theta)$ is given. R is the distance between the boron atom and the argon atom, or the center of the nitrogen molecule, θ is the angle between the 3-fold axis of BF_3 and the line along which R is measured. In all cases, the vertical axis gives the ratio of the local density of the liquid relative to the system density. In $g(R)$ the local density is averaged over a spherical shell of radius R and thickness ΔR, centered around the boron atom, while for $g(R,\theta)$, averaging occurs over a toruslike body formed by revolving the elementary surface bound by the directions θ and $\theta + \Delta\theta$, and by the distances R and $R + \Delta R$, around the 3-fold axis C_3 of BF_3. The angle θ ranges from 0 to 90°, so that both sides of the BF_3 molecule have to be integrated separately.

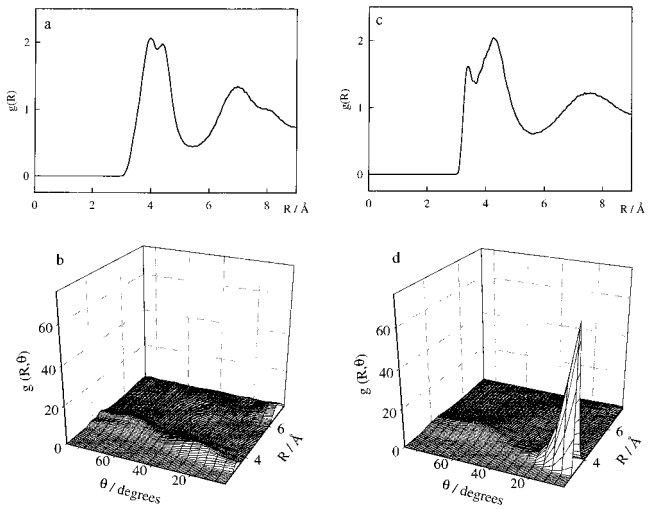

Figure 1. Monte Carlo probability distribution functions describing the solvation of boron trifluoride dissolved in liquefied argon (a, b) and in liquified nitrogen (c, d) at 88 K.

It may be anticipated that specific interactions of BF_3 with solvent molecules take the form of the van der Waals molecules between the species as found in the vapor phase and as calculated by ab initio. These, as said above, have the solvent molecule, Ar or N_2 centered on C_3 of BF_3. At $\theta = 0$, the integrating volume used in $g(R,\theta)$ is reduced to an elementary body centered around C_3. It follows that a concentration of solvent atoms near C_3 will be more clearly visible in $g(R,\theta)$, and panels b and d of Figure 1 reveal important differences in this region between the LAr and LN_2 simulations.

For LAr, $g(R,\theta)$ shows a ridge running roughly parallel with the θ axis, the maximum of which for $\theta = 0$ occurs at $R =$ 3.39 Å. This ridge is the first solvation shell of argon atoms around the BF_3 molecule. The dip in the ridge near $\theta = 50°$ reflects a slightly preferential solvation of BF_3 along its 3-fold axis.

For values of θ approaching 90°, the ridge splits into two. At $\theta = 90°$, the maximum at lower R represents argon atoms of the first shell lying in the BF_3 plane midway between two lines starting in the B atom and passing through different fluorine atoms, while the maximum at higher R represents atoms lying on, or near, such lines.

The radial distribution function $g(R)$ (Figure 1a) also clearly shows the first sovation shell. Its double maximum corresponds to the splitting of the ridge in $g(R,\theta)$. Integration of the first

(36) Allen, M. P.; Tildesley, D. J. *Computer Simulation of Liquids*; Clarendon Press: Oxford, 1987; p 21.

(37) Schmidt, M. W.; Baldridge, K. K.; Boatz, J. A.; Elbert, S. T.; Gordon, M. S.; Jensen, J. H.; Koseki, S.; Matsunaga, N.; Nguyen, K. A.; Su, S. J.; Windus, T. L.; Dupuis, M.; Montgomery, J. A. *J. Comput. Chem.* **1993**, *14*, 1347.

(38) Stone, A. J. *The Theory of Intermolecular Forces*; Clarendon Press: Oxford, 1996.

(39) Price, S. L.; Stone, A. J.; Alderton, M. *Mol. Phys.* **1984**, *52*, 987.

Table 6. Analysis of the Coordination of BF_3 in LN_2 and in LN_2/LAr Mixtures As Calculated by Monte Carlo Simulation[a]

	integration I: 4.25 Å, 30°			integration II: 4.25 Å, 35°		
	BF_3	1:1	1:2	BF_3	1:1	1:2
LN_2 (88 K)	1.1	26.6	72.3	0.4	17.7	81.9
Temperature Study of a 50% LAr/50% LN_2 Mixtures						
88 K	10.8	38.9	50.3	6.2	35.7	58.1
98 K	23.3	51.9	24.8	15.5	51.0	33.5
108 K	35.5	48.1	16.4	27.0	50.4	22.6

[a] All values given in percent.

shell gives an average of 14.5 argon atoms. In $g(R)$ as well as in $g(R,\theta)$ the second solvation shell is also visible. Integration shows that it is occupied by 46.6 argon atoms.

The two-dimensional distribution function for the LN_2 simulation is given in Figure 1d. At high values of θ, a ridge appears in $g(R,\theta)$ which resembles that of Figure 1b and which is due the nitrogen molecules in the first solvation shell. Although less clear than for LAr, here the ridge also splits into two near $\theta = 90°$. At low values of θ, however, a sharp maximum in the local density is observed: for LAr, in the direction $\theta = 0°$, the local density at the maximum in $g(R,\theta)$ equals 3.5; for LN_2, the value of the maximum is 71.1. Such a high local density is very uncharacteristic for a normal solvation shell and must be the consequence of the formation of more permanent associations between BF_3 and N_2. We identify these associations with van der Waals complexes. In the following paragraphs we will demonstrate that the N_2 molecules contained in the sharp peak of Figure 1d show characteristics compatible with van der Waals molecules, supporting their identification.

The number of N_2 molecules concentrated along C_3 was determined by counting all molecules inside two cones centered on C_3, one on each side of the BF_3 molecule, that lie within a limiting distance R from the boron atom. Figure 1d shows that, at $R = 4.25$ Å, the local density is reduced to a very low value: this distance was used as limiting distance. The choice of the opening angle θ of the cones is somewhat more arbitrary. Therefore, two integrations, once using $\theta = 30°$ and once with $\theta = 35°$, were made. The resulting values, translated into average coordinations, are 1.81 and 1.83, respectively. It is clear that at these values of θ the integration has sufficiently converged. The resulting value is very close to 2, suggesting that at 88 K BF_3 in LN_2 occurs predominantly as 1:2 complexes, with one N_2 on each side of the BF_3 molecule.

The analysis can be taken a step further by counting separately the number of configurations in which 0, 1, or 2 (this is one on each side of BF_3) N_2 molecules are present in the cones: in this way a partitioning between BF_3 monomers and 1:1 and 1:2 complexes is obtained. The resulting fractions, given in the top line of Table 6, indeed show the dominance of 1:2 complexes.

Figure 1c gives the radial distribution function $g(R)$ for the solution in LN_2. The intense peak of $g(R,\theta)$ is now seen as the sharp band at 3.32 Å. Its intensity is relatively low, due to the averaging over a spherical shell. The much broader band with a maximum at 4.23 Å is the first solvation shell. Thus, in $g(R)$ also, the important difference between N_2 molecules in the solvation shell and those attributed to van der Waals molecules is obvious.

As mentioned above, the isolated complex $BF_3 \cdot N_2$ has the C_∞ axis of N_2 aligned with C_3 of BF_3.[23] To see whether the N_2 molecules assigned to the van der Waals complexes in the simulation show the same structural characteristic, their angle

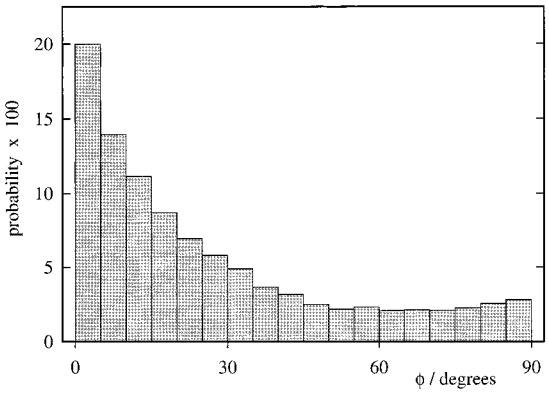

Figure 2. Monte Carlo probability distribution for the orientation of N_2 molecules van der Waals bonded to BF_3. The abscissa ϕ is the angle between the axis of N_2 and C_3 of BF_3.

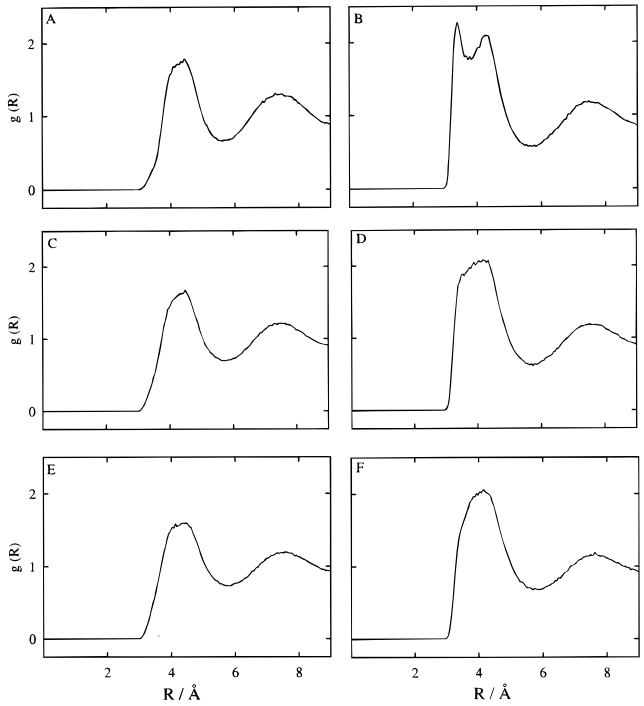

Figure 3. Monte Carlo radial distribution functions for solvation of BF_3 in a 50:50 Ar/N_2 mixture, as function of temperature. From top to bottom, the temperature of the simulation is 88, 98, and 108 K. At each temperature, the left panel gives the radial distribtion for Ar, the right panel for N_2.

ϕ with respect to C_3 was determined. A histogram of the results, giving the probability per 5° interval, is shown in Figure 2. Clearly, the largest fraction is found in the lowest interval, the fraction steadily decreasing toward higher ϕ. This is as expected for van der Waals complexes. The relatively important spread in the values of ϕ reflects the large amplitude deformations in ϕ that are typical for weak van der Waals complexes.

The population of van der Waals complexes in cryosolution is very sensitive to the temperature.[12−15] In view of the above assignment, it must be expected that the sharp band at 3.9 Å in $g(R)$ shows a similar temperature behavior. This was investigated by simulations of a 50:50 mixture of N_2 and Ar, at temperatures that fall within the interval of the experimental study, at 88, 98, and 108 K. The $g(R)$ for argon and for N_2 are shown in Figure 3. In a first count, the contents of the first solvation shell was determined by integrating $g(R)$ between $R = 0$ and $R = 5.8$ Å, without regard to the fact that some of the N_2 are involved in van der Waals molecules. In order of

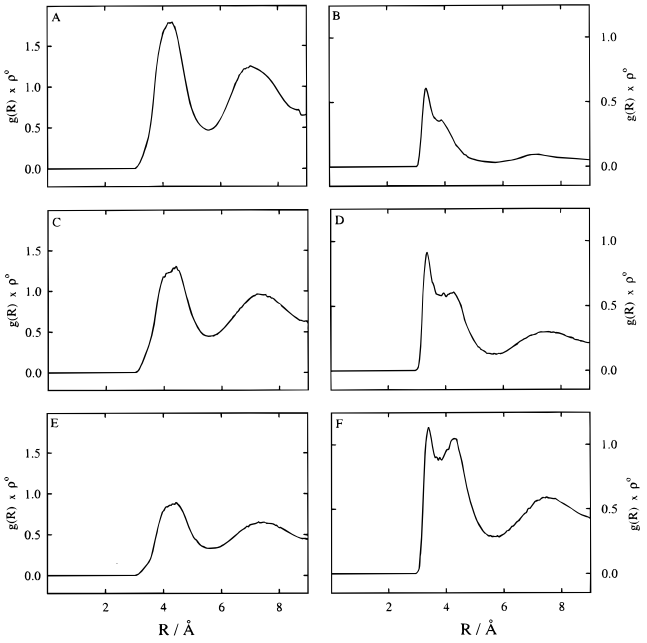

Figure 4. Monte Carlo solvation local densities around BF_3 in Ar/N_2 mixtures, as a function of concentration. From top to bottom, the mole fractions of N_2 are 0.08, 0.25, and 0.50. At each concentration, the left panel gives the local density for Ar, the right panel for N_2.

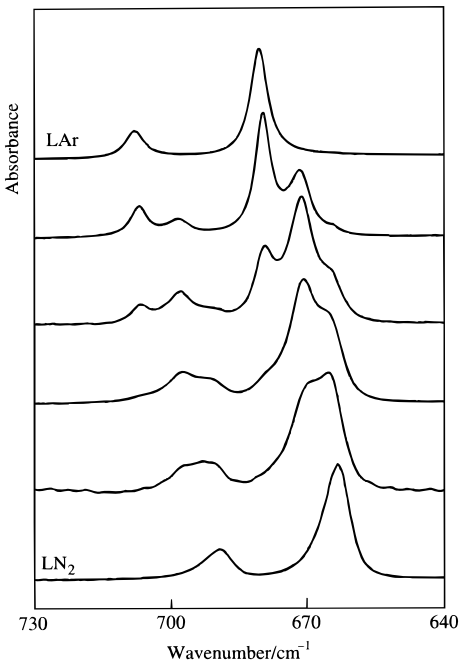

Figure 5. Infrared spectra in the $\nu_2^{BF_3}$ region of a solution of BF_3 in mixtures of Ar and N_2. The spectra were recorded at 86 K, and the mole fraction of BF_3 is 1×10^{-5}. From top to bottom, the mole fractions of N_2 in the solvent are 0.0, 0.2, 0.4, 0.6, 0.8, and 1.0.

increasing temperature, the values obtained for argon are 6.25, 5.75, and 5.52, and for nitrogen they are 7.89, 7.25, and 6.83. These data show that at each temperature there is an enrichment in nitrogen. This is attributed to the stronger interaction between BF_3 and N_2. With increasing temperature, the coordination numbers of argon and of nitrogen are seen to decrease; this is analogous to the trend experimentally observed for simple liquids.[40]

The evolution in the populations of monomers and 1:1 and 1:2 complexes in the temperature-dependent simulations was derived using the partitioning procedure described above. The results, also given in Table 6, indicate that with increasing temperature the fraction of 1:2 complexes steadily decreases, while that of monomers steadily increases. At the intermediate temperature, the decomposition of 1:2 complexes increases the fraction of 1:1 complexes, but at the highest temperature, the increased decomposition of the 1:1 complexes reduces its fraction. It will be shown below that this is in agreement with observations made in the IR spectra.

The populations of complexes are also influenced by the concentrations of the monomers. This was tested by performing simulations in which the fraction of nitrogen, compared to argon, was set at 8, 25, and 50%. The results are given in Figure 4 in the form of radial distribution functions for each species, multiplied by the system density of the same species. Thus, the height of the curves in these plots is linearly related to the local density. It can then be seen that, with increasing concentration of N_2, the fraction of complexes increases. At the same time, the number of N_2 molecules in the solvation shells increases, while their argon content decreases. All this is in line with expectations.

Vibrational Spectra. The behavior of BF_3 in LAr and LN_2 is illustrated in Figure 5, in which the region of $\nu_2^{BF_3}$ of the infrared spectra is given. The spectra were recorded at 86 K in a series of solvents in which the mole fraction x_{N_2} of nitrogen varies linearly between 0.0 and 1.0. It can be seen that the isotopic $^{10}B/^{11}B$ doublet red shifts by $\sim$17 cm^{-1} when the solvent is changed from LAr to LN_2. If the only interaction of the solute, BF_3, with the solvent is a nonspecific solvation, a gradual change in the solvent from pure LAr to pure LN_2 should cause the absorption bands to smoothly shift from their position in LAr to those in LN_2. However, the spectra in Figure 5 show a completely different evolution. At low fractions of N_2, on the low-frequency sides of the single bands observed in LAr, which we will call the A bands, new bands grow in. These, called B bands, are red shifted by $\sim$9 cm^{-1} from the corresponding A bands. With increasing N_2 fraction, the B bands increase and then decrease in relative intensity. At the same time, a third pair of bands emerges, red shifted by $\sim$17 cm^{-1} from the A bands, which we will call the C bands. Their relative intensity also increases with increasing N_2 fraction. In pure LN_2, at first sight only the C bands remain. Close inspection, however, shows that the band profiles are asymmetric. A least-squares band fitting using symmetric Gauss/Lorentz sum functions of the spectral region in Figure 5 is successful only when four bands are used to simulate the $\nu_2^{BF_3}$ region. The weak, extra two bands occur at frequencies compatible with those of the B bands. Thus, in LN_2, the A bands are absent, and the B bands are reduced to weak high-frequency shoulders on the C bands.

The above evolution in the spectra convincingly proofs the occurrence of specific interactions between BF_3 and N_2. When the A bands are assigned to solvated BF_3 monomers, in view of the Monte Carlo results, the B bands have to be assigned to solvated 1:1 complexes $BF_3 \cdot N_2$, and the C bands to solvated 1:2 complexes $N_2 \cdot BF_3 \cdot N_2$.

Solvent shifts on vibrational bands are also observed for solutes for which specific interactions with solvent atoms are unlikely. For such solutes, the vibrational bands in general occur at lower frequencies in LN_2 than in LAr, signaling that the attractive contributions to the solvent shift[41] are higher for LN_2 than for LAr. With increasing N_2 fraction, argon atoms in the first solvation shell are increasingly replaced by N_2 molecules.

(40) Karnicki, J. F.; Pings, C. J. In *Advances in Chemical Physics*; Prigogine, J., Rice, S. A., Eds.; Wiley: New York, 1976; Vol. XXXIV.

Table 7. Vibrational Frequencies (cm^{-1}) for BF_3, $BF_3{\cdot}N_2$, and $N_2{\cdot}BF_3{\cdot}N_2$ Observed in Liquefied Argon (85 K) and in Liquefied Nitrogen (85 K)

	LAr							
	monomer	1:1	$\Delta\nu_{exp}$	$\Delta\nu_{calc}$[a]	1:2	$\Delta\nu_{exp}$	$\Delta\nu_{calc}$[a]	LN_2
$\nu_1 + \nu_3(^{10}BF_3)$	2373.9	2370.8	−3.1					2369.5
ν^{N_2}	(2326)[b]	2330.1		+5.4	2330.1		+4.7	2330.9
$\nu_1 + \nu_3(^{11}BF_3)$	2323.9	2320.8	−3.1					2319.4
$\nu_3^{^{10}BF_3}$	1495.0	1493.1	−1.9	−3.2				1493.4
$\nu_3^{^{11}BF_3}$	1443.8	1441.9	−1.9	−3.2				1442.8
$\nu_1^{BF_3}$	(883.2)[c]	882.0	(−1.2)[c]	−2.6				
$\nu_2^{^{10}BF_3}$	707.0	697.9	−9.1	−19.0	690.1	−16.9	−35.8	691.2
$\nu_2^{^{11}BF_3}$	679.5	671.0	−8.5	−18.0	664.0	−15.5	−33.9	664.8

[a] Calculated using the ab initio values given in Table 2. [b] Taken from ref 46. [c] Calculated using the data for the ν_3 fundamental and the $\nu_1 + \nu_3$ combination band.

Due to the nonspecific contributions from the solvation shell, an increase in the N_2 fraction must induce a red shift of the solute's vibrational bands. This is indeed what is observed. For instance, at 86 K, the A band of $\nu_2^{^{11}BF_3}$ shifts from 680.4 cm^{-1} in pure LAr to 678.9 cm^{-1} in a 50/50 LAr/LN_2 mixture.

Comparison of the shifts of the B and C bands of $\nu_2^{BF_3}$ with those predicted by the ab initio calculations for the 1:1 and 1:2 complexes (Table 2) shows that the latter are overestimated by a factor of ~2. The fact that the experimental shifts are taken from solution spectra cannot fully account for this discrepancy. Thus, it appears that the normal coordinate-dependent contributions to the interaction energy are relatively poorly reproduced at this level of calculation.

The formation of complexes between BF_3 and N_2 is also observed in other regions of the spectra. The experimental data have been collected in Table 7. For $\nu_3^{BF_3}$ the B bands are shifted by −1.9 cm^{-1} from the monomer bands, while the predicted values (Table 2) are 3.2 cm^{-1}: the agreement is similar to that for the $\nu_2^{BF_3}$. The ab initio calculations predict that the bands of the 1:2 complex should be shifted from the 1:1 bands by a similar amount and, therefore, are expected to be separately observable. However, the B bands occur at frequencies at which the $\nu_3^{BF_3}$ are observed in LN_2, and no separate C bands are observed. This suggests that the B and C bands accidentally degenerate. As the predicted complexation shifts are small, it appears reasonable to assume that this discrepancy is due to differences in the nonspecific solvent effect on the $\nu_3^{BF_3}$ modes of $BF_3{\cdot}N_2$ and $N_2{\cdot}BF_3{\cdot}N_2$.

If the B and C bands are due to complexes, their relative intensities must decrease with increasing temperature of the solution. This is confirmed in Figure 6, where the $\nu_2^{BF_3}$ for a solution of BF_3 ($x_{BF_3} = 1 \times 10^{-5}$) in a 50:50 Ar/$N_2$ mixture is given at 88, 98, and 108 K. At 88 K, the spectrum is dominated by the C bands, with the A bands barely visible. At 108 K, the main maximum in each multiplet is due to the B band, with the A band more intense than the C band. The relative intensities of the components in each multiplet are related to the populations of the species and thus are amenable to a comparison with the Monte Carlo simulations. Because of the severe overlap of the B and C bands, no reliable relative intensities could be obtained from band fitting. Therefore, only a qualitative comparison with the simulation data is possible. To this end, in Figure 7 bar diagrams of the simulation results are given. The relative heights of the bars were obtained by multiplying the population fractions in Table 6 with the corresponding ab initio intensities and with the theoretical boron isotope abundance ratio. It can be seen that the bar diagrams neatly reproduce the evolution of the relative intensities in each multiplet.

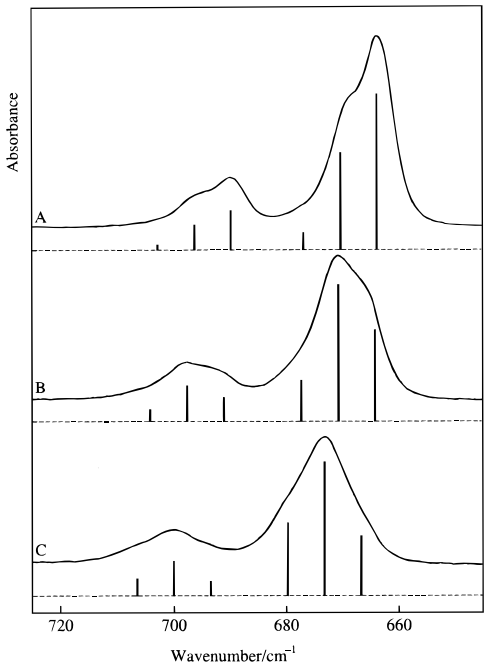

Figure 6. Infrared spectra in the $\nu_2^{BF_3}$ region of a solution of BF_3 in a 1:1 mixture of Ar and N_2. The temperatures of the solutions are 88 (A), 98 (B) and 108 K (C). The bar charts show the relative intensities predicted from the Monte Carlo simulations. In each triplet, and in order of decreasing frequency, the bars give the intensites for BF_3, $BF_3{\cdot}N_2$, and $N_2{\cdot}BF_3{\cdot}N_2$.

At each temperature, the main bar in each multiplet was positioned at the frequency of the maximum of the multiplet in the spectrum, the others were then positioned at intervals derived from the concentration study in Figure 5, and these intervals were assumed to be independent of temperature. The shifts in the positions of the bars in the diagrams, clearly visible in Figure 6, demonstrate the temperature dependence of the vibrational bands.

In Figure 7, the region of $\nu_1^{BF_3} + \nu_3^{BF_3}$ of a BF_3/N_2 mixture in LAr is shown at different temperatures. The broad background absorption in these spectra is the induced N_2 stretching mode, its width being caused by the nearly free rotation of the N_2 molecules in cryosolution.[42,43] The band at 2341 cm^{-1} is due

(41) Bulanin, M. O.; Orlova, N. D.; Zelikina, G. Ya. In *Molecular Cryospectroscopy*; Clark, R. J. H., Hester, R. E., Eds.; Advances in Spectroscopy 23; Wiley: Chichester, 1995; p 37.

(42) Kouzov, A. P. In *Molecular Cryospectroscopy*; Clark, R. J. H., Hester, R. E., Eds.; Advances in Spectroscopy 23; Wiley: Chichester, 1995; p 176.

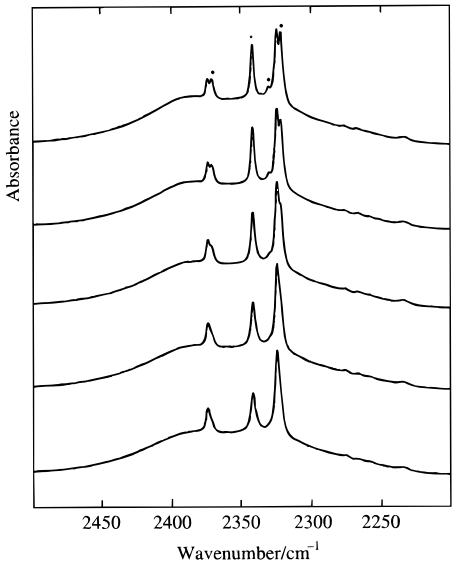

Figure 7. Infrared spectra in the $\nu_1^{BF_3} + \nu_3^{BF_3}$ region of a solution in LAr in which the mole fraction of BF_3 is 1×10^{-5} and the mole fraction of N_2 is 1.5×10^{-4}. From top to bottom, the temperature of the solution increases from 86 to 103 K.

to CO_2, which is present as an impurity in the Ar and N_2 gases used. The bands at 2373.9 and 2323.9 cm^{-1} are the A components of $\nu_1^{BF_3} + \nu_3^{BF_3}$; i.e., they are due to solvated BF_3 monomers. At lower temperatures, the corresponding B bands become clearly visible, at 2370.8 and 2320.8 cm^{-1}, respectively. At the concentrations of N_2 used to record the spectra, the intensity of the C bands is very low, and these bands cannot be distinguished in Figure 7.

The symmetric BF_3 stretching, $\nu_1^{BF_3}$, is symmetry-forbidden in infrared. In the 1:1 complex this mode, as is predicted in Table 2, acquires an IR intensity of 0.7 km mol^{-1}. Just as for BF_3·CO[27] and BF_3·CH_3F,[18] in solutions containing a large fraction of BF_3·N_2, a weak band is found in the expected region, at 882 cm^{-1}, which is assigned to $\nu_1^{BF_3}$. If we neglect the changes upon complexation in the cubic and higher terms in the force field of BF_3, the complexation shift of a combination band equals the sum of the shifts of the fundamentals. If we apply this to the shifts for $\nu_1^{BF_3} + \nu_3^{BF_3}$, using the experimental shifts for $\nu_3^{BF_3}$, a complexation shift of -1.2 cm^{-1} for $\nu_1^{BF_3}$ in BF_3·N_2 is derived. This value compares favorably, at the same level of accuracy as for the other modes, with the ab initio shift of -2.6 cm^{-1}

The complexation enthalpy for BF_3·N_2 was determined using a solution containing BF_3 ($x_{BF_3} = 1 \times 10^{-5}$) and N_2 ($x_{N_2} = 1.5 \times 10^{-4}$). At this concentration of N_2, the first solvation shells of all species involved contain mainly argon atoms. Hence, the enthalpy obtained in this study is essentially the value in LAr, ΔH°_{LAr}. Spectra of the solution were recorded between 86 and 103 K, and the Van't Hoff isochore was used to obtain ΔH°_{LAr}.[15]. The analysis requires intensities of a band of each of the species in the equilibrium, i.e., BF_3, N_2 and BF_3·N_2. For N_2 the choice is limited to the fundamental mode near 2350 cm^{-1}. This region, as can be seen in Figure 7, is disturbed by the presence of bands due to CO_2 and BF_3. As a consequence, no accurate intensities could be obtained for N_2. In view of the excess of N_2 used, its concentration throughout the temperature study hardly changes and was, therefore, treated as a constant. Intensities for BF_3 and BF_3·N_2 were obtained from a least-squares fit band fitting, using Gauss/Lorentz sum functions, of the spectral region in which the A, B, and C components appear with the highest separation, i.e., the region of $\nu_2^{BF_3}$. This region, at the temperatures used, is shown in Figure 8. Errors introduced by resolution of the bands due to N_2·BF_3·N_2 from those of BF_3·N_2 were largely avoided by using a very low concentration of N_2. As can be seen in Figure 8, the bands of the 1:2 complex then are weak in comparison to those of the 1:1 complex, so that uncertainties introduced by the band fitting are negligible. The Van't Hoff plot of $\ln[I(BF_3{\cdot}N_2)/I(BF_3)]$ versus $1/T$ is shown in Figure 9. From the slope of the linear regression through the experimental points, corrected for the expansion of the solution,[44] ΔH°_{LAr} was found to be $-4.8(5)$ kJ mol^{-1}.

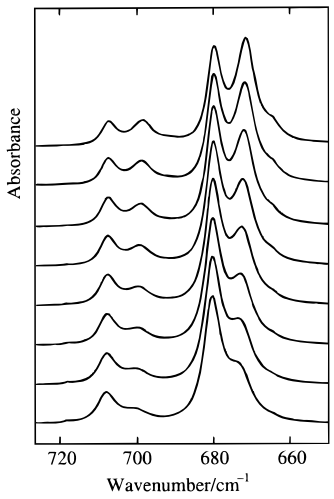

Figure 8. Infrared spectra in the $\nu_2^{BF_3}$ region of a solution in LAr in which the mole fraction of BF_3 is 1×10^{-5} and the mole fraction of N_2 is 1.5×10^{-4}. From top to bottom, the temperature of the solution increases from 86 to 103 K.

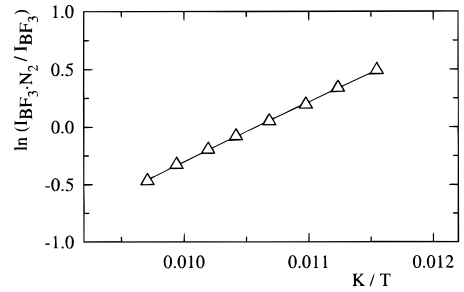

Figure 9. Van't Hoff plot for the BF_3·N_2 van der Waals complex dissolved in liquid argon.

In principle this method could be used to measure ΔH°_{LAr} for the 1:2 complex as well. This requires experimental conditions under which the bands due to the 1:2 complex have substantial relative intensity. Then, as observed above, the least-squares resolution of the bands leads to unacceptable integrated intensities. Therefore, the measurement of ΔH°_{LAr} for N_2·BF_3·N_2 was abandoned.

The ΔH°_{LAr}. of the 1:1 complex obtained here cannot straightforwardly be compared with the ab initio complexation energy. Therefore, the enthalpy was transformed into a complexation energy by the method described before.[16] In a first step, the solvent stabilizations of the species involved were estimated by SCRF/SCIPCM calculations[7,11] at the RHF/6-31+G* level, treating the solvent as pure LAr. The stabilizations obtained are 4.13, 0.24, and 2.88 kJ mol^{-1} for BF_3, N_2,

(43) Temkin, S. I.; Steele, D. A. *J. Phys. Chem.* **1996**, *100*, 1996.

(44) Van der Veken, B. J.; *J. Phys. Chem.* **1996**, *100*, 17436.

and $BF_3 \cdot N_2$, respectively. Treating these stabilizations as enthalpies, they were used to correct the liquid-phase enthalpy, transforming it into a vapor phase complexation enthalpy, ΔH°_{gas}. The resulting value is $-6.3(5)$kJ mol^{-1}. Using standard statistical thermodynamics[45] the zero point vibrational and thermal contributions to the enthalpy were calculated at the midpont of the temperatures interval in which ΔH°_{gas} was measured, using the ab initio rotational constants and vibrational frequencies. These contributions were then used to transform ΔH°_{LAr} into a complexation energy. This results in a complexation energy of $-7.3(10)$ kJ mol^{-1}. The uncertainty quoted has been chosen as twice the value on ΔH°_{LAr} to account for the approximations made. The experimental result is significantly lower than the ab initio value of -12.18 kJ mol^{-1}. Apparently, the ab initio calculations overestimate the stability complex. When the ab initio result is corrected for basis set superposition error, the underestimated value of -4.61 kJ mol^{-1} is obtained. This shows that the basis set superposition correction should be balanced by the basis set saturation correction. Previous experience with BF_3, however, has shown that even significantly larger basis sets do not lead to a converged saturation correction.[19] Therefore, no attempts were made to refine the ab initio calculations.

Conclusions

In this work, cryosolutions of BF_3, using Ar and N_2 as solvents, have been studied by Monte Carlo simulations and by infrared spectroscopy. The results from both approaches can be interpreted as showing the formation of van der Waals complexes $BF_3 \cdot N_2$ and $N_2 \cdot BF_3 \cdot N_2$ when N_2 is present in the solution. Ab initio calculations show that the 1:2 complex can be formed. A qualitative comparison shows that the relative populations of monomers, and 1:1 and 1:2 complexes predicted by the simulations account very well for the relative intensities observed in the infrared. This, evidently, lends support to the interpretation put forward in this study.

It was observed in the Introduction that the ΔH° for complexes of various Lewis bases with BF_3 measured in LAr are more negative by some 4.5 kJ mol^{-1} than those in LN_2. The ΔH°_{LAr} for $BF_3 \cdot N_2$ obtained in this study, $-4.8(5)$ kJ mol^{-1}, is nearly equal to this difference. This shows that the smaller enthalpy in LN_2 is almost completely accounted for by the fact that a van der Waals bond between boron and a solvent N_2 molecule must be broken before the new complex bond can be formed.

Acknowledgment. W.A.H. is indebted to the Fund for Scientific Research (FWO, Belgium) for an appointment as Postdoctoral Fellow. The FWO is also thanked for financial help toward the spectroscopic equipment used in this study. Support by the Flemish Community, through the Special Research Fund (BOF), is gratefully acknowledged. Dr. E. J. Sluyts is thanked for recording spectra in the early stages of this study.

JA980626D

(45) Knox, J. H. *Molecular Thermodynamics. An Introduction for Chemists*; Wiley: London, 1971.

(46) Moore, D. S.; Schmidt, S. C.; Shaw, M. S. *J. Chem. Phys*. **1994**, *101*, 3488.